Lipid Bilayer Domain Fluctuations as a Probe of Membrane Viscosity

Brian A. Camley
Department of Physics, University of California, Santa Barbara, California 93106, USA

Cinzia Esposito and Tobias Baumgart
Department of Chemistry, University of Pennsylvania, Philadelphia, Pennsylvania, 19104

Frank L. H. Brown
Department of Chemistry and Biochemistry, University of California, Santa Barbara, California 93106, USA and
Department of Physics, University of California, Santa Barbara, California 93106, USA

We argue that membrane viscosity, η_m, plays a prominent role in the thermal fluctuation dynamics of micron-scale lipid domains. A theoretical expression is presented for the timescales of domain shape relaxation, which reduces to the well known $\eta_m = 0$ result of Stone and McConnell in the limit of large domain sizes. Experimental measurements of domain dynamics on the surface of ternary phospholipid and cholesterol vesicles confirm the theoretical results and suggest domain flicker spectroscopy as a convenient means to simultaneously measure both the line tension, σ, and η_m governing the behavior of individual lipid domains. **Correspondence: camley@physics.ucsb.edu or flbrown@chem.ucsb.edu**

As a first step to understanding the biophysics of plasma membranes [1], model membrane systems have been developed to mimic aspects of biomembranes under controlled, simplified laboratory conditions [2]. Much work has focused on vesicles composed of ternary phospholipid/cholesterol mixtures, where physical properties of lipid domains can be characterized by fluorescence microscopy [3–6].

Among the most biologically important physical properties of inhomogeneous membrane systems are the line tension between coexisting phases σ and the membrane viscosity η_m. Line tensions influence the distribution of domain sizes [7], and viscosities set diffusion coefficients for lipid domains [8] and membrane proteins [9]. Measurements of line tension via microscopy are well known, particularly for lipid monolayers [10–12]; recent "domain flicker spectroscopy"[6] experiments were developed to measure the line tension on the surface of ternary vesicles. The membrane viscosity is not as simple to measure, though it may be estimated by fitting diffusion coefficients to the Saffman-Delbrück form [8, 13] or by microrheology [14].

In this letter we show that flicker spectroscopy may be used to measure not only σ, but also η_m. Our theoretical work exploits hydrodynamic analysis introduced by Stone and McConnell (SM) [15], but extends their results to a physical regime where membrane viscosity is relevant. Our experiments show that domain relaxation times do deviate from the $\eta_m = 0$ SM predictions. By combining theory with experiment, it becomes possible to directly measure η_m.

Our analysis of domain fluctuations assumes an isolated domain of constant area within a large flat membrane (Fig. 1). We assume that the boundary energy is given by $E = \sigma L$, with σ the line tension and L the domain perimeter. It is convenient, theoretically [15] and experimentally [6, 11], to express the domain shape in Fourier modes, $r(\theta, t) = R(1+\frac{1}{2}\sum_{n\neq 0} u_n(t)e^{in\theta})$, with n from $-N/2$ to $N/2$. To second order in $u_n(t)$, the energy cost of deviations from the minimum energy circle with radius R is [6]

$$\Delta E = \frac{\sigma\pi R}{2}\sum_{n=2}^{N/2}(n^2-1)|u_n|^2. \tag{1}$$

The equipartition theorem (as applied to the Fourier components of a real-valued physical quantity [16]) immediately leads to the spectrum of equilibrium shape fluctuations [11],

$$\langle |u_n|^2\rangle = \frac{2k_BT}{\sigma\pi R(n^2-1)} \tag{2}$$

and a direct experimental route to the determination of σ via measurement of $\langle |u_n|^2\rangle$ [6].

The time-dependence associated with fluctuations in $u_n(t)$ may be calculated within the hydrodynamic model introduced by Saffman and Delbrück (SD) [9], namely a single thin flat fluid sheet with surface viscosity η_m surrounded by a bulk fluid of viscosity η_f treated within the creeping-flow approximation (Fig. 1) [17]. This picture neglects the dual leaflet structure of the bilayer and applies only to symmetric bilayers with domains that are in registry across both leaflets. The available experimental [19], theoretical [20] and simulation [21] evidence suggests that domain registry is nearly perfect in ternary model membrane systems, with inter-leaflet domain mismatch confined to areas of tens of lipids for an entire domain [20, 21]. The SD picture is expected to be completely adequate to describe domain dynamics over the optical length-scales observed experimentally.

Relaxation of a general domain shape is driven by the line tension σ, with the radially directed force per unit length at the

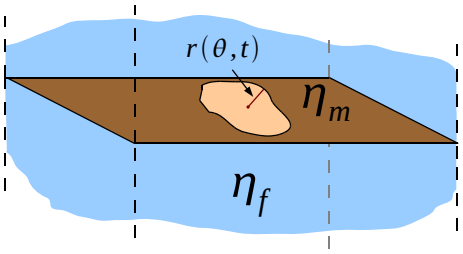

FIG. 1: The shape of a quasi-circular lipid domain within a thin, flat membrane is specified by the distance from the domain center of mass to the boundary as a function of the polar angle θ. Both lipid phases are assumed to share the surface viscosity η_m [17]; the membrane is surrounded by a bulk fluid of viscosity η_f.

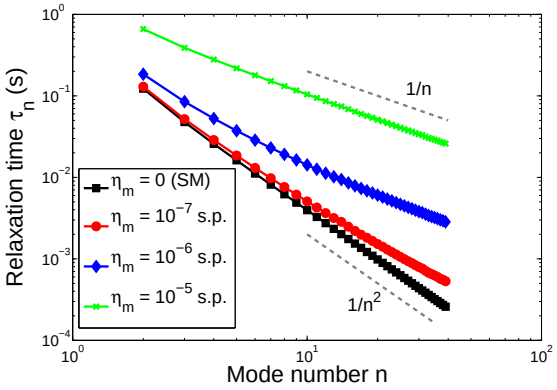

FIG. 2: Relaxation times (Eq. 5)as a function of mode number for several membrane viscosities assuming a domain with $R = 2.5\mu$m, $\sigma = 0.1$ pN, and η_f = 0.01 Poise (water). As membrane viscosity is increased, the relaxation times increase, and the scaling with n changes from $\tau_n \sim n^{-2}$ for $R/n >> L_{sd}$ (Eq. 7) to $\tau_n \sim n^{-1}$ for $R/n << L_{sd}$ (Eq. 8).

domain boundary given by the functional derivative $f_r(\theta,t) = -R^{-1}\delta(\Delta E(t))/\delta r(\theta,t)$ [22], which is, to linear order in $u_n(t)$,

$$f_r(\theta,t) = -\frac{\sigma}{2R}\sum_{n=-N/2}^{N/2}(n^2-1)u_n(t)e^{in\theta} \equiv \frac{1}{2}\sum f_n(t)e^{in\theta}. \tag{3}$$

This force drives flow within the bilayer and in the bulk fluid. In particular, the radial velocity at the domain boundary $v_r(\theta,t) = \frac{d}{dt}r(\theta,t) = \frac{R}{2}\sum \dot{u}_n(t)e^{in\theta}$ may be obtained through application of the techniques of Stone and McConnell [15], or by use of the more general formalism developed by Lubensky and Goldstein [22]. The result is conveniently cast in terms of the Fourier modes [18]

$$v_n(t) = R\dot{u}_n(t) = \frac{n^2R}{\eta_m}I_n(\Lambda)f_n(t) \tag{4}$$

where the integral $I_n(\Lambda) = \int_0^\infty dx J_n^2(x)/\left[x^2(x+\Lambda)\right]$, $J_n(x)$ is a Bessel function of the first kind and $\Lambda = 2R\eta_f/\eta_m$. Combining Eqs. 3 and 4 leads to $\dot{u}_n(t) = -u_n(t)/\tau_n$ with the solution $u_n(t) = u_n(0)e^{-t/\tau_n}$ where

$$\tau_n = \frac{\eta_m R}{\sigma}\frac{1}{n^2(n^2-1)}\left[\int_0^\infty dx \frac{J_n^2(x)}{x^2(x+\Lambda)}\right]^{-1}. \tag{5}$$

The fluctuation-dissipation theorem [23] provides the connection between the relaxation of $u_n(t)$ and the equilibrium correlation functions measured in flicker spectroscopy,

$$\langle u_n(t)u_{-n}(0)\rangle = \langle|u_n|^2\rangle e^{-t/\tau_n}. \tag{6}$$

Eq. 5 is the primary theoretical result of this letter; the expression is evaluated for a few representative parameters in Fig. 2. Though there is no general closed-form solution for the integral in Eq. 5, it reduces to two simple results in appropriate limits.

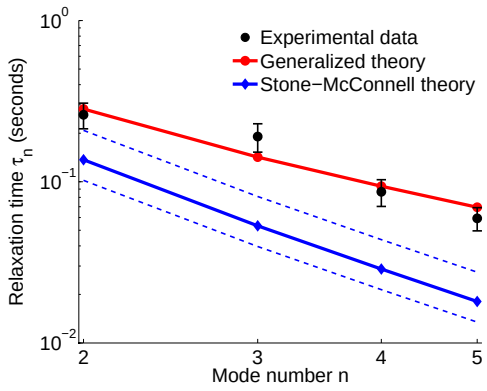

FIG. 3: DiPhyPC / Cholesterol / DPPC relaxation times for a single domain trace with $R = 3.8\mu$m. Error bars are 95% confidence intervals for the fit to Eq. 6. The fit membrane surface viscosity η_m is 3.25×10^{-6} s.p. Also plotted is the SM theory for the relaxation times (Eq. 7). The theoretical results assume $\sigma = 0.19$ pN, as extracted from the variance in u_n (Eq. 2); dotted lines represent uncertainty in the SM predictions from adjusting σ by one standard deviation. Uncertainty in σ can not account for the deviation between SM and experiment.

For large domains and sufficiently small n ($\Lambda >> n$), dissipation in the bulk fluid dominates the dynamics, η_m may be neglected, and Eq. 5 approaches a result generally attributed to Stone and McConnell (SM) [15, 24]

$$\tau_n^{\text{fluid}} = \frac{2\pi R^2 \eta_f}{\sigma} \frac{n^2 - 1/4}{n^2(n^2-1)}. \tag{7}$$

In the opposite limit ($\Lambda << n$), the membrane viscosity dominates and η_f may be neglected, recovering the result of Mann et al. [24]

$$\tau_n^{\text{membrane}} = \frac{4\eta_m R}{n\sigma}. \tag{8}$$

As both Eq. 7 and Eq. 8 neglect a source of dissipation, $\tau_n \geq \tau_n^{\text{membrane}}, \tau_n^{\text{fluid}}$. The crossover between regimes occurs where the wavelength of the fluctuations ($\sim R/n$) becomes comparable to the Saffman–Delbrück length scale $L_{sd} = \eta_m/2\eta_f$. Membrane viscosities generally fall within $(0.1 - 10) \times 10^{-6}$ surface poise (poise-cm, or grams/s) [8, 13, 25], leading to Saffman-Delbrück lengths $L_{sd} \sim 0.1 - 10$ microns. Recent experimental measurements [6] on domains with radii of a few microns are thus expected to deviate from the SM result (see Fig. 2), unlike the much larger domains originally studied by McConnell and co-workers [10, 15].

To test the above analysis, giant unilamellar vesicles of a ternary mixture of phospholipids [dipalmitoylphosphatidylcholine (DPPC) and diphytanoylphosphatidylcholine (DiPhyPC)] and cholesterol were studied experimentally using the flicker spectroscopy technique (see [6] for details). 28 $r(\theta, t)$ traces from individual domains were analyzed, each from a vesicle with 25:55:20 molar ratios of DiPhyPC / Chol. / DPPC at 20 ± 1°C [18]. (DiPhyPC was chosen over dioleoylphosphatidylcholine (DOPC) used in [6] for its greater photostability [26].) Domain images were thresholded to find $r(\theta, t)$, which was Fourier transformed to yield $u_n(t)$. Line tensions (σ) were extracted from the variance in Fourier modes u_n via Eq. 2 (with mean $\sigma = 0.23$ pN over all 28 traces) and relaxation times (τ_n) were determined by fitting $\langle u_n(t) u_{-n}(0) \rangle$ to single exponential decay. With σ, R and η_f known, Eq. 5 has a single unknown parameter: η_m. The relaxation times over all measured n values were simultaneously fit to our general result (Eq. 5) using η_m as the fit parameter. A typical fit is shown in Fig. 3. Applying this procedure to all traces determined the mean membrane surface viscosity $\eta_m = (4 \pm 1) \times 10^{-6}$ s.p., consistent with the low-temperature values observed from fitting diffusion constants. For comparison, Petrov and Schwille [13] use the data of Cicuta et al. [8] and find viscosities of $\approx 2 \times 10^{-6}$ s.p. at a similar temperature, though for different lipids. A similar analysis based on the SM expression for the τ_n (Eq. 7) was also attempted [18]. As SM neglects η_m, there are no free parameters in τ_n^{fluid} and relaxation times are predicted immediately from σ. The SM theory predicts relaxation times in clear disagreement with the measurements (Fig. 3); additional dissipation from the bilayer itself must be considered to explain the data. We note that prior successful fits of the SM theory to experimental results using DOPC / Cholesterol / DPPC lipid mixtures [6] were only apparent. Eq. 2 of the present work corrects Eq. 3 of [6]. Also, the extraction of τ_n from correlations in $u_n(t)$ (via Eq. 6) corrects the procedure of [6], which was based upon correlations in $|u_n(t)|^2$. Experimental relaxation times that appeared consistent with SM in [6] are actually four times longer than SM predictions when the analysis is carried out properly. This level of disagreement between SM and experiment is similar to results summarized in Fig. 3.

We have proposed a simple extension to the usual Stone-McConnell theory for relaxation times of domain fluctuations, Eq. 5, and have verified it against experimental data. The experimental results suggest that membrane viscosity significantly affects

these relaxation times for the smallest wavelength modes observable by microscopy. By combining equilibrium measurements of line tension (via. Eq. 2) with the measurement of dynamic relaxation, the viscosity of a lipid bilayer may be determined.

ACKNOWLEDGMENTS

This work was supported in part by the National Science Foundation (grant No. CHE-0848809). B.A.C. acknowledges the support of the Fannie and John Hertz Foundation.

[1] Gennis, R. B., 1989. Biomembranes: Molecular Structure and Function. Springer-Verlag, Berlin.
[2] Veatch, S. L., and S. L. Keller, 2005. Seeing spots: complex phase behavior in simple membranes. *Biochim. Biophys. Acta.* 1746:172.
[3] Dietrich, C., et al., 2001. Lipid rafts reconstituted in model membranes. *Biophys. J* 80:1417–1428.
[4] Samsonov, A. V., I. Mihalyov, and F. S. Cohen, 2001. Characterization of cholesterol-sphingomyelin domains and their dynamics in bilayer membranes. *Biophys. J* 81:1486–1500.
[5] Veatch, S. L., and S. L. Keller, 2003. Separation of Liquid Phases in Giant Vesicles of Ternary Mixtures of Phospholipids and Cholesterol. *Biophys. J.* 85:3074.
[6] Esposito, C.,A. et al., 2007. Flicker Spectroscopy of Thermal Lipid Bilayer Domain Boundary Fluctuations. *Biophys. J.* 93:3169.
[7] Frolov, V., et al., 2006. "Entropic traps" in the kinetics of phase separation in multicomponent membranes stabilize nanodomains. *Biophys. J.* 91:189.
[8] Cicuta, P., S. L. Keller, and S. L. Veatch, 2007. Diffusion of Liquid Domains in Lipid Bilayer Membranes. *J. Phys. Chem. B* 111:3328.
[9] Saffman, P. G., and M. Delbrück, 1975. Brownian motion in biological membranes. *Proc. Nat. Acad. Sci. USA* 72:3111.
[10] Benvegnu, D. J., and H. M. McConnell, 1992. Line tensions between liquid domains in lipid monolayers. *J. Phys. Chem.* 96:6820–6824.
[11] Goldstein, R. E., and D. P. Jackson, 1994. Domain Shape Relaxation and the Spectrum of Thermal Fluctuations in Langmuir Monolayers. *J. Phys. Chem.* 98:9626–9636.
[12] Alexander, J.C., et al., 2007. Domain relaxation in Langmuir films. *J. Fluid Mech.* 571:191–219.
[13] Petrov, E. P., and P. Schwille, 2009. Translational Diffusion in Lipid Membranes beyond the Saffman-Delbruck Approximation. *Biophys. J.* 94:L41.
[14] Harland, C., M. Bradley, and R. Parthasarathy, 2010. Microrheology of freestanding lipid bilayers. *Biophys. J.* 98:76a.
[15] Stone, H. A., and H. M. McConnell, 1995. Hydrodynamics of quantized shape transitions and lipid domains. *Proc. Royal Society of London A* 448:97.
[16] Safran, S. A., 2003. Statistical Thermodynamics of Surfaces, Interfaces, and Membranes. Westview Press.
[17] If the viscosities of the domain and its surroundings differ, η_m is approximately the mean of the two viscosities [18].
[18] See supplementary material for further details
[19] Collins, M. D., and S. L. Keller, 2008. Tuning lipid mixtures to induce or suppress domain formation across leaflets of unsupported asymmetric bilayers *PNAS* 105:124.
[20] Collins, M. D., 2008. Interleaflet Coupling Mechanisms in Bilayers of Lipids and Cholesterol *Biophys. J.* 94:L32.
[21] Risselada, H. J., and S. J. Marrink, 2008. The molecular face of lipid rafts in model membranes *PNAS* 105:17367.
[22] Lubensky, D. K., and R. E. Goldstein, 1996. Hydrodynamics of monolayer domains at the air-water interface. *Phys. Fluids* 8:843.
[23] Chandler, D., 1987. Introduction to Modern Statistical Mechanics. Oxford, New York.
[24] Mann, E. K., et al., 1995. Hydrodynamics of domain relaxation in a polymer monolayer. *Phys. Rev. E* 51:5708.
[25] Dimova, R., et al., 1999. Falling ball viscosimetry of giant vesicle membranes: Finite-size effects. *Eur. Phys. J. B* 12:589.
[26] Honerkamp-Smith, A. R., et al., 2008. Line Tensions, Correlation Lengths, and Critical Exponents in Lipid Membranes Near Critical Points. *Biophys. J.* 95:236.

Supplementary material for "Lipid Bilayer Domain Fluctuations as a Probe of Membrane Viscosity"

Supplement A. DETAILS ON THE DERIVATION OF THE SHAPE RELAXATION TIMES

Our calculation of the relaxation times is based on the work of both Stone and McConnell [1] and Lubensky and Goldstein [2]; indeed, our results follow immediately from the hydrodynamic analysis presented in these works with only slight modifications. The mathematical details are summarized here, elaborating upon the treatment in Appendix C of [2]. Within the Saffman-Delbrück picture of a fluid membrane sheet [3], it is possible to predict the in-plane velocity of all points on the membrane surface for an arbitrary distribution of in-plane forces acting on the membrane [2, 3]. Given a force density $\mathbf{F}(\mathbf{r})$ (per unit area), the membrane velocity is calculated from the membrane Green's function tensor $T_{ij}(\mathbf{r})$ for velocity response to an applied point force,

$$v_i(\mathbf{r}) = \int d\mathbf{r}' T_{ij}(\mathbf{r}-\mathbf{r}')F_j(\mathbf{r}'). \tag{A1}$$

Here, and in all that follows, the indices i and j refer to in-plane cartesian directions (x or y), with summation implied in expressions with repeated indices. Although there is no simple closed-form expression for T_{ij}, it may be expressed as the integral [2]

$$\begin{aligned} T_{ij}(\mathbf{r}) &= \frac{-1}{2\pi\eta_m}\int_0^\infty \frac{dq}{q^2(q+1/L_{sd})}\left[\frac{r_i r_j}{r^3}qJ_0'(qr) + \left(\delta_{ij}-\frac{r_i r_j}{r^2}\right)q^2 J_0''(qr)\right] \\ &= \frac{-1}{2\pi\eta_m}\int_0^\infty \frac{dq}{q^2(q+1/L_{sd})}\left[-\left(\delta_{ij}-\frac{r_i r_j}{r^2}\right)J_0(qr)q^2 + \left(\delta_{ij}-2\frac{r_i r_j}{r^2}\right)J_1(qr)\frac{q}{r}\right] \end{aligned} \tag{A2}$$

where $L_{sd} = \eta_m/(2\eta_f)$, η_m is the membrane surface viscosity, η_f is the bulk fluid viscosity, and J_n are Bessel functions of the first kind (the primes indicate differentiation). We emphasize that this result differs slightly from the form used in [2]. The bilayer geometry considered in this work requires $2\eta_f$ to appear in the denominator of L_{sd} whereas the monolayer geometry at the air-water interface considered in [2] places η_f (without the factor of 2) in this constant. The bilayer is subject to dissipation from the bulk fluid both above and below the bilayer, which accounts for the factor of 2 [4, 5].

Our result for domain fluctuation dynamics is calculated in the limit of linear response, considering only small fluctuations of domain shape away from the minimum energy configuration of a perfect circle of radius R. These small fluctuations in domain shape give rise to restoring forces, which are explicitly written in Eq. 3 of the main paper. The important point about this expression, is that the force vanishes for the undeformed circle - only linear (and, in principle, higher order) contributions are present. In order for the velocity of Eq. A1 to be linearly dependent on the shape deformations, the Green's function must be evaluated for the undeformed domain geometry of the perfect circle. Any deviations from the zeroth order geometry in T_{ij} would necessarily lead to second (and higher) order contributions in the velocity when multiplied against the forces. We are thus led to a less general form of expression A1, which considers the velocity of the domain boundary at points (R,θ) as driven by restoring forces at points (R,θ') in polar coordinates.

$$v_i(R,\theta) = \int_0^\infty dr' r' \int_0^{2\pi} d\theta'\, T_{ij}(R\hat{\mathbf{r}}(\theta)-\mathbf{r}')\delta(r'-R)f_r(\theta')\hat{r}_j'(\theta') = R\int_0^{2\pi} d\theta'\, T_{ij}\left(R\hat{\mathbf{r}}(\theta)-R\hat{\mathbf{r}}'(\theta')\right)f_r(\theta')\hat{r}_j'(\theta'). \tag{A3}$$

The unit vectors $\hat{\mathbf{r}}(\theta) = (\hat{r}_x(\theta),\hat{r}_y(\theta)) = (\cos\theta,\sin\theta)$ and $\hat{\mathbf{r}}'(\theta') = (\hat{r}_x(\theta'),\hat{r}_y(\theta')) = (\cos\theta',\sin\theta')$ point along the outward radial direction for the indicated polar angles. The radially directed velocity is then given by $v_r(\theta) = \hat{\mathbf{r}}(\theta)\cdot\mathbf{v}(R,\theta)$ so that

$$\begin{aligned} v_r(\theta) &= R\int_0^{2\pi} d\theta'\,\hat{r}_i(\theta)\left(T_{ij}\left(R\hat{\mathbf{r}}(\theta)-R\hat{\mathbf{r}}'(\theta')\right)f_r'(\theta')\hat{r}_j'(\theta')\right. \\ &\equiv \int_0^{2\pi} d\theta' R T_{\hat{\mathbf{r}}\hat{\mathbf{r}}'}\left(R\hat{\mathbf{r}}(\theta)-R\hat{\mathbf{r}}'(\theta')\right)f_{r'}(\theta') \end{aligned} \tag{A4}$$

The velocities and forces are defined explicitly in the main paper. If the radial velocity is measured at angle θ on the circle, as driven by a radially directed force at angle θ', the cartesian vector separating these two points is $\mathbf{r}-\mathbf{r}' = R(\cos\theta-\cos\theta',\sin\theta-\sin\theta')$ with a separation of $\mathcal{R} = |\mathbf{r}-\mathbf{r}'| = 2R\sin(\frac{\theta-\theta'}{2})$. It is clear by symmetry that the Green's function for radially directed forces and velocities $T_{\hat{\mathbf{r}}\hat{\mathbf{r}}'}\left(R\hat{\mathbf{r}}(\theta)-R\hat{\mathbf{r}}'(\theta')\right)$ can only depend on the angles θ and θ' via their difference $\theta-\theta'$; a rotation of both

points around the origin will not affect value of the radially directed Green's function on the circle. Carrying out the calculation explicitly, starting from Eq. A2 leads to

$$\begin{aligned} T_{\hat{\mathbf{r}}\hat{\mathbf{r}}'}(\theta-\theta') &\equiv T_{\hat{\mathbf{r}}\hat{\mathbf{r}}'}\left(R\hat{\mathbf{r}}(\theta)-R\hat{\mathbf{r}}'(\theta')\right) = \frac{-1}{2\pi\eta_m}\int_0^\infty \frac{dq}{q^2(q+1/L_{sd})}\left[-\cos^2\left(\frac{\theta-\theta'}{2}\right)J_0(q\mathcal{R})q^2+\frac{J_1(q\mathcal{R})q}{\mathcal{R}}\right] \\ &= \frac{-1}{2\pi\eta_m}\int_0^\infty \frac{dq}{q^2(q+1/L_{sd})}\left\{-\cos^2\left(\frac{\theta-\theta'}{2}\right)J_0\left[2qR\sin\left(\frac{\theta-\theta'}{2}\right)\right]q^2+\frac{J_1\left[2qR\sin\left(\frac{\theta-\theta'}{2}\right)\right]q}{2R\sin\left(\frac{\theta-\theta'}{2}\right)}\right\} \\ &= \frac{-1}{2\pi\eta_m}\int_0^\infty \frac{dx}{x^2(x+R/L_{sd})}\left\{-\cos^2\left(\frac{\theta-\theta'}{2}\right)J_0\left[2x\sin\left(\frac{\theta-\theta'}{2}\right)\right]x^2+\frac{J_1\left[2x\sin\left(\frac{\theta-\theta'}{2}\right)\right]x}{2\sin\left(\frac{\theta-\theta'}{2}\right)}\right\}. \\ &= \frac{-1}{2\pi\eta_m}\int_0^\infty \frac{dx}{x^2(x+R/L_{sd})}\left\{\frac{\partial^2}{\partial(\theta-\theta')^2}J_0\left[2x\sin\left(\frac{\theta-\theta'}{2}\right)\right]\right\}. \end{aligned} \tag{A5}$$

This expression may be substituted into Eq. A4 to yield

$$v_r(\theta) = \int_0^{2\pi} d\theta' R T_{\hat{\mathbf{r}}\hat{\mathbf{r}}'}(\theta-\theta')f_{r'}(\theta') \tag{A6}$$

which has the form of a simple convolution in the polar angle around the domain perimeter, so that

$$v_n(t) = \pi\mathcal{T}_n f_n(t) \tag{A7}$$

$$\mathcal{T}_n \equiv \frac{R}{\pi}\int_0^{2\pi} d\theta e^{-in\theta}T_{\hat{\mathbf{r}}\hat{\mathbf{r}}'}(\theta) = \frac{R}{\pi}\int_0^{2\pi} d\theta\cos(n\theta)T_{\hat{\mathbf{r}}\hat{\mathbf{r}}'}(\theta) \tag{A8}$$

and the final equality originates from the fact that $T_{\hat{\mathbf{r}}\hat{\mathbf{r}}'}(\theta)$ is even around the point $\theta=\pi$, which is clear from symmetry considerations as well as the explicit mathematical expressions. The integral over θ is taken using the last line of Eq. A5 and applying integration by parts twice to move the derivatives off the Bessel function and on to $\cos(n\theta)$. The boundary terms vanish.

$$\begin{aligned} \mathcal{T}_n &= \frac{n^2R}{2\pi^2\eta_m}\int_0^\infty \frac{dx}{x^2(x+R/L_{sd})}\int_0^{2\pi} d\theta\cos(n\theta)J_0\left[2x\sin\left(\frac{\theta}{2}\right)\right] \\ &= \frac{n^2R}{\pi^2\eta_m}\int_0^\infty \frac{dx}{x^2(x+R/L_{sd})}\int_0^{\pi} d\phi\cos(2n\phi)J_0\left[2x\sin\phi\right] \\ &= \frac{n^2R}{\pi\eta_m}\int_0^\infty \frac{dxJ_n(x)^2}{x^2(x+R/L_{sd})}. \end{aligned} \tag{A9}$$

The final integral over θ may be found in standard tables [6]. Eq. A9 and Eq. A7 lead immediately to Eq. 5 of the main paper.

Supplement B. THE MEANING OF η_m WHEN DOMAIN AND SURROUNDINGS DO NOT SHARE THE SAME VISCOSITY

For future reference, we restate Eq. 5 from the main paper

$$\tau_n = \frac{\eta_m R}{\sigma}\frac{1}{n^2(n^2-1)}\left[\int_0^\infty dx\frac{J_n^2(x)}{x^2(x+R/L_{SD})}\right]^{-1} = \frac{\eta_m R}{\sigma}\frac{1}{I_n(2R\eta_f/\eta_m)n^2(n^2-1)}. \tag{B1}$$

This expression and its derivation above are restricted to the case that both the domain and its surroundings have identical surface viscosity, η_m. Though we are not able to present a fully general theory for the case where domain viscosity η_d differs from the surrounding viscosity η_s, we can argue that that the measured quantity η_m (obtained via fitting data to Eq. B1) is approximately equal to the mean viscosity $(\eta_d+\eta_s)/2$, when the experimental data is observed to fit the form of Eq. B1. We can also place bounds on the accuracy of this approximation.

In the limiting case where dynamics are governed solely by the behavior within the membrane, it is known that Eq. 8 of the main paper may be generalized to the case of distinct η_d and η_s [7]

$$\tau_n^{\text{membrane}} = \frac{2(\eta_d+\eta_s)R}{n\sigma}. \tag{B2}$$

In this limit, the correspondence mentioned above is exact. Measuring mode relaxation times and fitting to paper Eq. 8 yields $\eta_m = (\eta_d + \eta_s)/2 \equiv \bar{\eta}$. More generally, for any finite mode number n, the experimental relaxation times will always be longer than τ_n^{membrane} of eq. B2 owing to the additional dissipation afforded by the surrounding bulk solvent. Since we assume that the available experimental data is well fit by eq. B1 this means that

$$\frac{\eta_m R}{\sigma} \frac{1}{I_n(2R\eta_f/\eta_m)n^2(n^2-1)} > \frac{2(\eta_d+\eta_s)R}{n\sigma} \tag{B3}$$

where η_m must now be interpreted as a fitting parameter or effective viscosity that incorporates the influence of both η_d and η_s. The influence of solvent decreases with increasing n and hence approaches equality most closely for the largest mode number measured in a given experiment n_{max}. This inequality may be rearranged and considering only n_{max} yields the tightest bound on $\bar{\eta}$ possible from the experimental measurements

$$\begin{aligned} \bar{\eta} &< \alpha\eta_m \\ \alpha &\equiv \frac{n_{max}}{4I_n(2R\eta_f/\eta_m)n_{max}^2(n_{max}^2-1)}. \end{aligned} \tag{B4}$$

The dimensionless quantity $\alpha > 1$ provides a measure for how closely mode n_{max} approaches the idealized "membrane only" limit. Values of α close to one are nearly in the limiting regime whereas larger values correspond to systems more strongly influenced by the bulk solvent. The domains analyzed in this work span the range of $\alpha = 1.1 - 2.1$.

We also note that the measured relaxation time for mode n will always be shorter than that for a hypothetical membrane with homogeneous viscosity $\eta_{lim} = \max\{\eta_s, \eta_d\}$, because such a membrane is subject to additional dissipation over the region of the membrane that has been replaced by higher viscosity. For a given value of $\bar{\eta}$, the largest value that η_{lim} can possibly assume is $2\bar{\eta}$, which would correspond to the membrane having one region (either domain or surroundings) with vanishing viscosity. If we assume Eq. B1 provides a good fit to the data (with η_m the measured fit constant) then the preceding argument implies that $\tau_n(\eta_m) < \tau_n(2\bar{\eta})$, by which we mean

$$\frac{\eta_m R}{\sigma} \frac{1}{I_n(2R\eta_f/\eta_m)n^2(n^2-1)} < \frac{2\bar{\eta}R}{\sigma} \frac{1}{I_n(R\eta_f/\bar{\eta})n^2(n^2-1)} \tag{B5}$$

Since $\tau_n(\eta)$ increases monotonically with η, this expression implies

$$\eta_m < 2\bar{\eta} \tag{B6}$$

Combing Eq. B4 and Eq. B6 leads to bounds on the value of the mean bilayer viscosity $\bar{\eta}$ in terms of the measured effective viscosity η_m

$$\frac{\eta_m}{2} < \bar{\eta} < \alpha\eta_m. \tag{B7}$$

This expression quantifies the meaning of our prior assertion that $\eta_m \sim \bar{\eta}$. As noted above, the experimental data considered in this work involves domains with α values on the order of two or smaller and so $\frac{\eta_m}{2} < \bar{\eta} < 2\eta_m$ provides a conservative estimate of the uncertainty in our measurement of $\bar{\eta}$. To within a factor of two, $\eta_m = \bar{\eta}$.

We stress that Eq. B7 does not preclude the possibility that $\eta_m = \bar{\eta}$, since $\alpha > 1$ for measurement of any finite n. The equality does hold in the limit of large n and it is possible that this equality extends over all n. Indeed, if perfect experimental data extending over all n values were found to fit Eq. B1, it would necessarily be the case that $\eta_m = \bar{\eta}$ since the equality must hold at high n, thus setting the value for the entire set of modes. The preceding analysis accounts for the possibility that the agreement between Eq. B1 and experiment may only be apparent/approximate due to uncertainty in the data. Without data extending down to the $\alpha = 1$ limit, it is not possible to surmise that the functional form of B1 with a constant η_m value holds over all n values.

Supplement C. DETAILS OF THE COMPARISON BETWEEN THEORY AND EXPERIMENT

Eq. B1 predicts the R dependence of relaxation times for mode n. The form of this expression suggests a natural collapse of the data onto a single dimensionless curve for each mode

$$\frac{\sigma\tau_n}{\eta_m L_{sd}} = g_n(R/L_{sd}) \tag{C1}$$

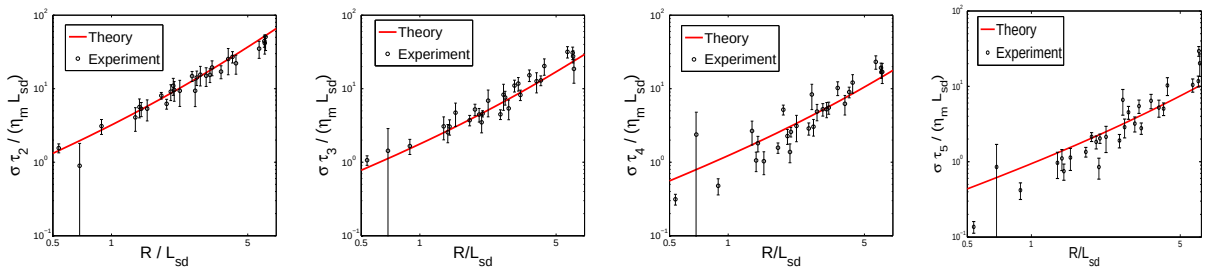

(a)n=2 (b)n=3 (c)n=4 (d)n=5

FIG. 1: Rescaling relaxation times collapses the data to the form predicted by the extended theory, Eq. C1. Error bars are propagated from the uncertainty in the measured quantities τ_n and σ. The experimental data closely matches the theoretical predictions.

where $g_n(y) = \frac{1}{n^2(n^2-1)} y \left[\int_0^\infty dx \frac{J_n^2(x)}{x^2(x+y)}\right]^{-1}$. Since the experimental data is collected from domains with a continuous range of R, but only a few discrete n values, Eq. C1 provides an appealing theoretical prediction to assess the validity of the proposed theoretical model over the full range of collected experimental data.

We note that Eq. C1 contains four distinct physical parameters that contribute to τ_n: σ, η_m, η_f and R. We assume three of these quantities to be known from measurements other than the relaxation time. The viscosity of water, η_f, is well known. The line tension of the domain is known from the equilibrium fluctuations as described in the main paper and the domain radius is known from direct observation. The values of R and σ do vary from domain to domain and so analysis of the decay times is necessarily carried out individually for each domain. After determining the domain boundary $r(\theta, t)$ as in the paper and extracting the deviations from circular shape, $u_n(t)$, we fit the autocorrelation functions $\langle u_n(t) u_{-n}(0)\rangle$ to the form $\langle |u_n|^2\rangle e^{-t/\tau}$ to determine the relaxation times for each observable mode (n=2,3,4,5). (Here, and in all subsequent fits, we use MATLAB's implementation of the Levenberg-Marquardt algorithm for nonlinear least-squares.) We then fit these four modes simultaneously to Eq. B1 to determine the single best fit η_m for each domain. Since η_m represents the best fit to the behavior of the entire domain, and not a single mode, the measured quantities $\tau_n^{experimental}$ will generally differ from the $\tau_n^{predicted}$ obtained by inserting σ, η_m, η_f and R into Eq. B1; the magnitude and nature of the deviations provide an estimate of the fit quality afforded by Eq. B1 to the experimental data. In Figs. 1 and 2 we present two different visualizations of the quality-of-fit obtained by the theoretical model proposed in the present work (Eq. B1). Fig. 1 plots the measured relaxation times, rescaled to the dimensionless form suggested by Eq. C1. The experimental data is in very good agreement with the theoretical predictions. The deviations between experiment and theory that do exist for individual points appear to be non-systematic, i.e. they are equally apparent over all mode numbers and for all domain radii and the scatter falls on both sides of the theoretical predictions. (It could be argued that the theory for mode $n = 5$ does show some systematic deviations from the data, however the $n = 5$ data is right at the limit of experimental resolution for many domains and this data may not be fully reliable. The analysis discussed in this section was also carried out using only modes $n = 2, 3, 4$ and no significant changes were observed.)

Alternatively, we can simply plot the ratio between the measured relaxation times and the relaxation times predicted by Eq. B1

$$\tau_n^{\text{experimental}} / \tau_n^{\text{predicted}} = \frac{\tau_n^{\text{experimental}}}{\eta_m R} \sigma n^2(n^2-1) \int_0^\infty dx \frac{J_n^2(x)}{x^2(x+\Lambda)}. \tag{C2}$$

If the experimental data carried no uncertainties and Eq. B1 served as a perfect description of physical reality, this quantity would equal unity for all n and for all domains. The data plotted in this form is given in Fig. 2. Although we see scatter just as in the representation of Fig. 1, the agreement between theory and experiment is perhaps more striking here - the data points straddle the theoretical predictions and show no systematic trends in the deviations that are observed.

By contrast to the above, if we attempt to explain the experimental measurements by fitting to the Stone-McConnell form with a similar procedure, using the bulk solvent viscosity as the independent fit parameter, we see much worse results. In this case we assume Eq. 7 of the main paper is the correct model for the dynamics

$$\tau_n^{fluid} = \frac{2\pi R^2 \eta_f}{\sigma} \frac{n^2 - 1/4}{n^2(n^2-1)}. \tag{C3}$$

We use the same procedure outlined above to determine the τ_n's from experiment, and find the best fitting value of the *bulk viscosity* η_f for each domain (as previously, the domain radius R and line tension σ are known from the thermal fluctuations) by fitting to modes $n = 2, 3, 4, 5$ simultaneously. If Eq. C3 were a good model for the system's dynamics, the ratio

$$\frac{\sigma \tau_n^{experimental}}{2\pi R^2 \eta_f} \frac{n^2(n^2-1)}{n^2 - 1/4} = \tau_n^{experimental} / \tau_n^{fluid} \tag{C4}$$

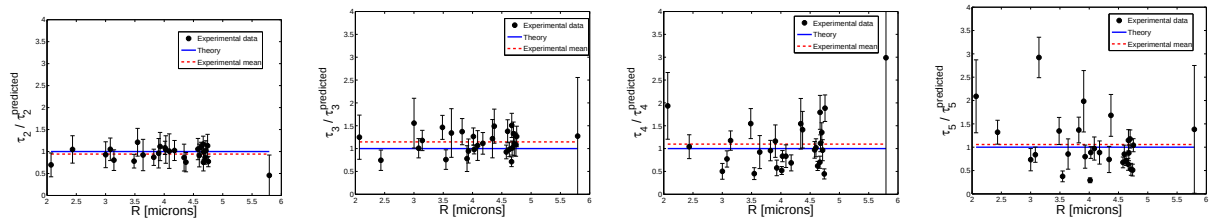

(a)n=2 (b)n=3 (c)n=4 (d)n=5

FIG. 2: No strong systematic error is seen in using Eq. B1 to "predict" observed data from the best fit viscosity. As in Fig. 1, error bars are propagated from the uncertainty in the measured quantities τ_n and σ. The dashed red line simply measures the average taken over all the experimental points in each plot. The proximity of this line to one for all n indicates there is very little, if any, systematic error associated with the predicted expression (Eq. B1).

should be close to one for all domain radii and all mode numbers n. In fact, what we find is that the $n = 2$ mode relaxation times are systematically low, while the times for $n = 3$, $n = 4$, and $n = 5$ are systematically long (Fig. 3), with the disagreement becoming more pronounced as n gets larger. This systematic deviation is predicted by Eq. B1. To demonstrate this, we generate

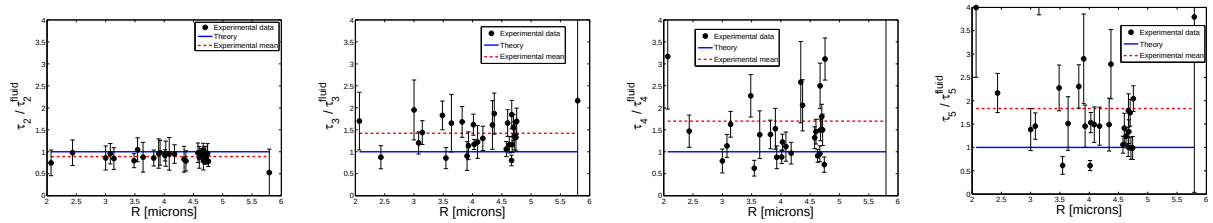

(a)n=2 (b)n=3 (c)n=4 (d)n=5

FIG. 3: Attempting to fit experimental data to the Stone-McConnell theory, using a different bulk viscosity for each domain, causes systematic problems; $n = 2$ relaxation times are systematically low compared to the best fit, and $n = 3, 4, 5$ are increasingly large compared to the best fit.

relaxation times from Eq. B1 for domains in the range $R = 2 - 5$ microns, with a membrane surface viscosity $\eta_m = 3 \times 10^{-6}$ s.P., bulk fluid viscosity of $\eta_f = 1$ cP and line tension $\sigma = 0.2$ pN. This manufactured "data" was fit to the Stone-McConnell form using the above procedure (Fig 4). The results are in striking agreement with Fig. 3 - the best fit $n = 2$ times are below theoretical predictions, whereas modes $n = 3, 4, 5$ show the opposite behavior. Even the magnitudes of the average deviations are close to the experimental plot. The Stone-McConnell theory fails in a manner completely consistent with the fact that the experimental data agrees with the predictions of Eq. B1.

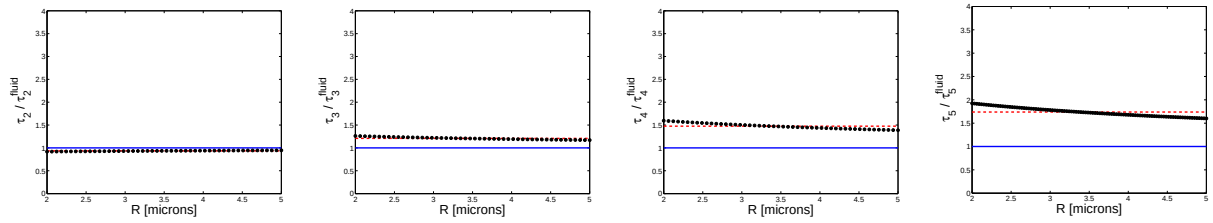

(a)n=2 (b)n=3 (c)n=4 (d)n=5

FIG. 4: Attempting to fit relaxation times given by Eq. B1 to the Stone-McConnell form (using η_f as the fit parameter) generates systematic deviations similar to those observed experimentally (Fig. 3).

In summary, we have shown that our prediction (Eq. B1) provides a globally satisfactory fit to the experimental data. The theory does a good job reproducing experiment over a range of domain sizes and all observable mode numbers with a single fit parameter (η_m) used to describe each domain. By contrast, the Stone-McConnell theory provides an unsatisfactory fit to the

experimental results. Furthermore, the errors seen in the SM fits are predicted by our theoretical analysis and are fully consistent with an experimental system that behaves in accord with Eq. B1. Although we have ruled out the Stone-McConnell theory as an adequate description of the experiments solely on the basis of the data, we feel an even stronger case against this model is the fact that it requires one to assume bulk solvent viscosities that vary from domain to domain with values as high as 3 cP or three times higher than the known viscosity of water at the experimental temperatures (see the next section). It is sensible that individual domains sampled from different vesicles may have different membrane surface viscosities and line tensions since the lipid stoichiometry is variable from vesicle to vesicle and each domain thus represents a distinct physical system from the perspective of the bilayer. The bulk solvent surrounding the bilayer however is constant from domain to domain. It is impossible to reconcile the experimental data with the Stone-McConnell form (Eq. C3), either from the physical or statistical perspectives.

Supplement D. ADDITIONAL DATA

We present twelve additional data traces, to indicate the quality of fits involved (Fig. 5). Each of the plots is similar to Fig. 3 of the main paper, which is seen to be in no way extraordinary in comparison to the behavior of other domains. In each of these, the solid blue line indicates the Stone-McConnell result with $\eta_f = 1$ centipoise (cP), and line tension as determined from the equilibrium measurement. The experimental relaxation times are almost universally significantly longer than the Stone-McConnell prediction. The red line indicates the best fit to our general form, Eq. B1, with the line tension given by the equilibrium measurements. The best fit value of the membrane surface viscosity, as well as the equilibrium line tension, are given in each figure. Plotted in green is the best fit to the Stone-McConnell form by adjusting the bulk solvent viscosity; the required bulk viscosities range from 130% to 300% of the known value of 1 cP at 20° C. Also, the deviations observed in Fig. 3 can be seen; the Stone-McConnell result does not have the correct slope to fit the observed data, though this is more apparent in aggregate (as in the preceding section) than in any individual trace.

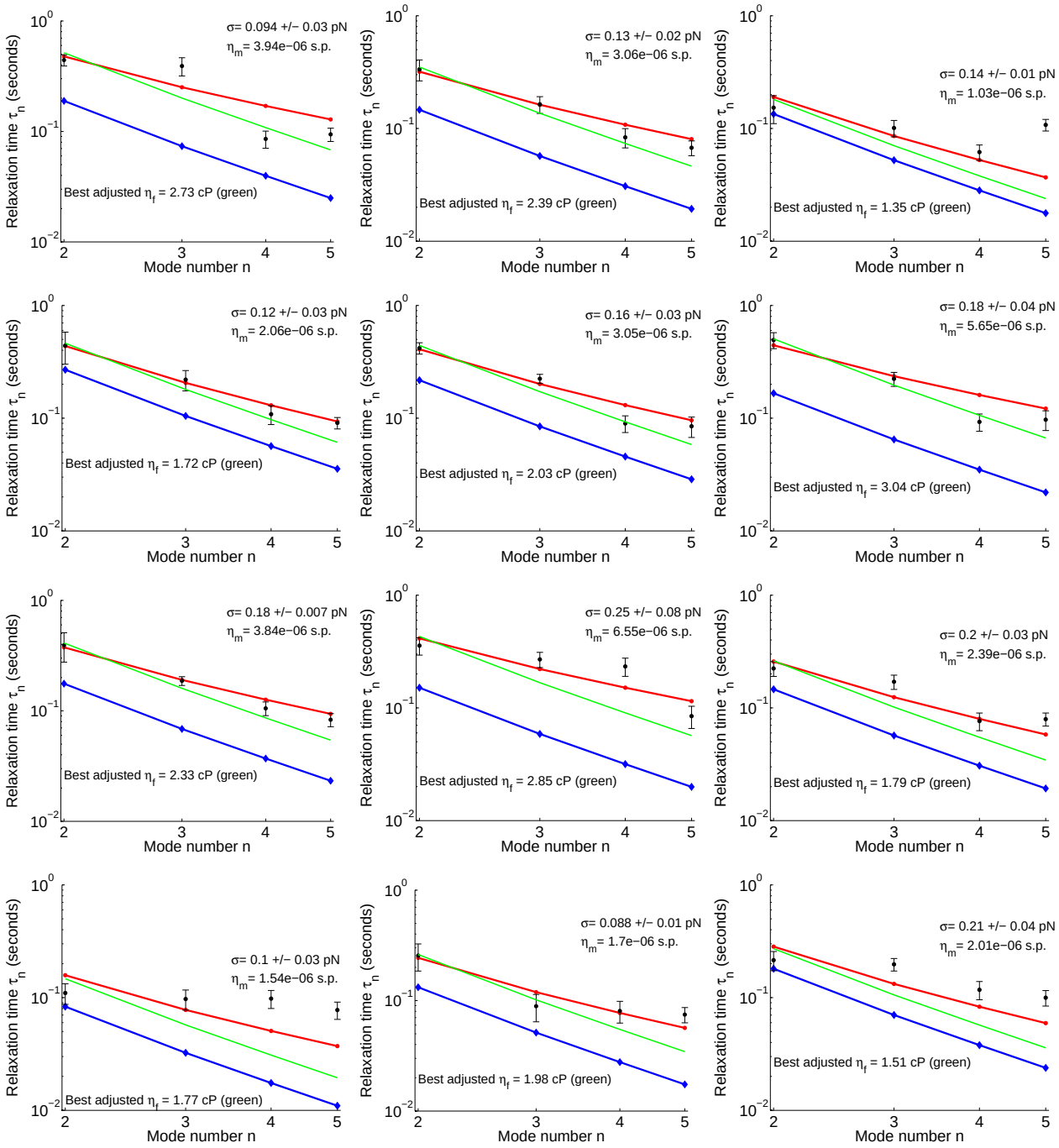

FIG. 5: Data from additional domains.

[1] H. A. Stone and H. M. McConnell, Proc. Royal Society of London A **448**, 97 (1995).
[2] D. K. Lubensky and R. E. Goldstein, Phys. Fluids **8**, 843 (1996).
[3] P. G. Saffman and M. Delbrück, Proc. Nat. Acad. Sci. USA **72**, 3111 (1975).
[4] P. G. Saffman, J. Fluid. Mech. **73**, 593 (1976).
[5] N. Oppenheimer and H. Diamant, Biophys. J. **96**, 3041 (2009).
[6] I. S. Gradshteyn and I. M. Ryzhik, *Table of Integrals, Series, and Products* (Academic Press, San Diego, 1994), 5th ed.
[7] E. K. Mann, S. Hénon, D. Langevin, J. Meunier, and L. Léger, Phys. Rev. E **51**, 5708 (1995).